



OPEN ACCESS

EDITED BY

Xin Wang,
National Institutes of Health (NIH),
United States

REVIEWED BY

Shuai Zhang,
Tianjin University of Traditional Chinese
Medicine, China
Yuliang Feng,
University of Oxford, United Kingdom
Weiwei Qi,
Zhongshan School of Medicine, Sun
Yat-sen University, China

*CORRESPONDENCE

Zhao Yin,
zhaoyin@stu2014.jnu.edu.cn
Jingjun He,
hjjs2@126.com
Junzhang Tian,
jz.tian@163.com

[†]These authors have contributed equally
to this work

SPECIALTY SECTION

This article was submitted to Molecular
Diagnostics and Therapeutics,
a section of the journal
Frontiers in Molecular Biosciences

RECEIVED 06 June 2022

ACCEPTED 08 July 2022

PUBLISHED 08 August 2022

CITATION

Liu F, Tang L, Li Q, Chen L, Pan Y, Yin Z,
He J and Tian J (2022), Single-cell
transcriptomics uncover the key
ferroptosis regulators contribute to
cancer progression in head and neck
squamous cell carcinoma.
Front. Mol. Biosci. 9:962742.
doi: 10.3389/fmolb.2022.962742

COPYRIGHT

© 2022 Liu, Tang, Li, Chen, Pan, Yin, He
and Tian. This is an open-access article
distributed under the terms of the
[Creative Commons Attribution License
\(CC BY\)](https://creativecommons.org/licenses/by/4.0/). The use, distribution or
reproduction in other forums is
permitted, provided the original
author(s) and the copyright owner(s) are
credited and that the original
publication in this journal is cited, in
accordance with accepted academic
practice. No use, distribution or
reproduction is permitted which does
not comply with these terms.

Single-cell transcriptomics uncover the key ferroptosis regulators contribute to cancer progression in head and neck squamous cell carcinoma

Fei Liu^{1†}, Lindong Tang^{2†}, Qing Li^{3†}, Leihui Chen³, Yuyue Pan³,
Zhao Yin^{4*}, Jingjun He^{1*} and Junzhang Tian^{1*}

¹Cancer Screening Center, Department of Health Management, Guangdong Second Provincial General Hospital, Guangdong, China, ²Institute of Hematology School of Medicine Jinan University, Guangdong, China, ³Department of Stomatology Guangdong Second Provincial General Hospital, Guangdong, China, ⁴Department of Hematology Guangdong Second Provincial General Hospital, Guangdong, China

The mechanism underlying the association between the development of head and neck squamous cell carcinoma (HNSCC) and ferroptosis is unclear. We analyzed the transcriptomes of 5902 single cells from a single-cell RNA-sequencing (scRNA-seq) dataset. They then aggregate into B cells, epithelial cells, fibroblasts, germ cells, mesenchymal cells, cancer stem cells, stem cells, T cells and endometrial cells, respectively. Our study shows that multiple pathways are significantly enriched in HNSCC development including extracellular matrix structural components, humoral immune responses, and muscle contraction. Differentially expressed genes analysis in Pseudotime analysis, pathway and biological function indicated that there was a significant correlation in the ferroptosis pathway. Furthermore, higher ferroptosis potential index (FPI) scores were significantly associated with worse overall survival prognosis in HNSCC patients. Pseudo-temporal, survival analyses and immunohistochemistry identified multiple central genes in HNSCC development, including ACSL1, SLC39A14, TFRC, and PRNP genes, and indicated associated ferroptosis. Overall, our study detected ferroptosis-related features is closely correlated with HNSCC prognosis and development, and deserved candidates suitable for immunotherapy treatment strategies determination for HNSCC patients.

KEYWORDS

head and neck squamous cell carcinoma, cell heterogeneity, ferroptosis, prognostic, single cell RNA sequencing

Introduction

Head and neck squamous cell carcinoma (HNSCC), which is frequently encountered in the clinical setting, is the seventh leading cause of cancer-related death worldwide: approximately 700,000 new cases and 350,000 deaths were reported worldwide in 2018 (Membreno et al., 2021; Sacco et al., 2021). HNSCC mainly includes cancers of the nasal cavity, paranasal sinus, oral cavity, pharynx, and throat, and over 90% of these cancers are squamous cell carcinomas (Jing et al., 2021; Membreno et al., 2021). Although there have been continuous advances in the field of comprehensive surgery, radiotherapy, and chemotherapy in recent years, the 5-year survival rate of HNSCC has not significantly improved, and 30–40% of patients are likely to develop distant metastasis within 5 years (Membreno et al., 2021). Moreover, 58% of patients may have advanced disease (stage III to IV) when they are first diagnosed, and this is a great challenge to treatment (Hamman et al., 2021). In order to improve the diagnosis and treatment of this cancer, it is important to understand the cellular mechanisms involved in its progression and metastasis (Hamman et al., 2021; Membreno et al., 2021).

Ferroptosis is a newly discovered form of programmed cell death characterized by iron-dependent lethal accumulation of lipid peroxides (lipid reactive oxygen species or lipid ROS) that was recently identified as one of the mechanisms of cancer cell death in several cancers, including liver cancer, kidney cancer, bone cancer, and lung cancer (Chen et al., 2022; Peng et al., 2023). Ferroptosis occurs when the levels of lipid ROS exceed the cellular antioxidative threshold and oxidative stress overload is induced in cells (Zhang et al., 2022). Excess oxidative stress causes damage to large molecules such as proteins, nucleic acids, and lipids, and eventually leads to cell injury or death (Zhai et al., 2022). With regard to cellular morphology, ferroptosis is characterized by loss of membrane integrity with morphologically normal nuclei and shrunken mitochondria as well as thickening of the mitochondrial double membranes and rupture of the outer mitochondrial membrane (Zhang et al., 2022).

Ferroptosis was first discovered in the study of the lethal mechanisms of the small molecule drug erastin against tumor cells carrying a mutation of the oncogene RAS (Liang et al., 2019). Erastin can bind to voltage-dependent anion channel-2/3 of mitochondria to induce ferroptosis of cancer cells. Erastin can also inhibit the function of the cystine/glutamate antiporter system to reduce intracellular glutathione levels, resulting in the accumulation of lipid ROS to induce ferroptosis. In addition, a series of artificial compounds, such as RSL3, DPI7, DPI10, DPI12, and DPI13, can inhibit glutathione peroxidase-4, and thereby increase the levels of peroxides in cancer cells, leading to Fe²⁺-dependent metabolic abnormalities (Yang and Stockwell, 2016). Translational research has shown that the chemotherapeutic drug sorafenib can also suppress the cystine/glutamate antiporter system to trigger cell ferroptosis in several cancers (Cao and Dixon, 2016). Furthermore, low-dose sorafenib can induce ferroptosis, but high-dose sorafenib can induce not only ferroptosis, but also other forms of programmed

cell death (Peng et al., 2023). Xie et al. (2022), investigating the transcriptome data of TCGA and Chinese Glioma Genome Atlas (CGGA) database, and thus identifying 36 radiosensitivity- and 19 ferroptosis associated differentially expressed genes with a prognostic value. In results, they also revealed that the radiosensitivity- and ferroptosis-associated biomarkers, includes HSPB1, STAT3, CA9, MAP1LC3A, MAPK1, ZEB1, and TNFAIP3, with a prognostic value for gliomas patients. Huang et al. (2022), found that the ferroptosis therapy can be a effectively approach to trigger the cancer cell death, and thus activating the cell oxidative phosphorylases and promoting cell oxidative damage. Magesh and Cai (Forthcoming 2022), revealed that the ferritin play an important susceptor for abnormal mitochondrial function, metabolism and oxidative phosphorylation in tumor cells, and also a target for tumor therapy.

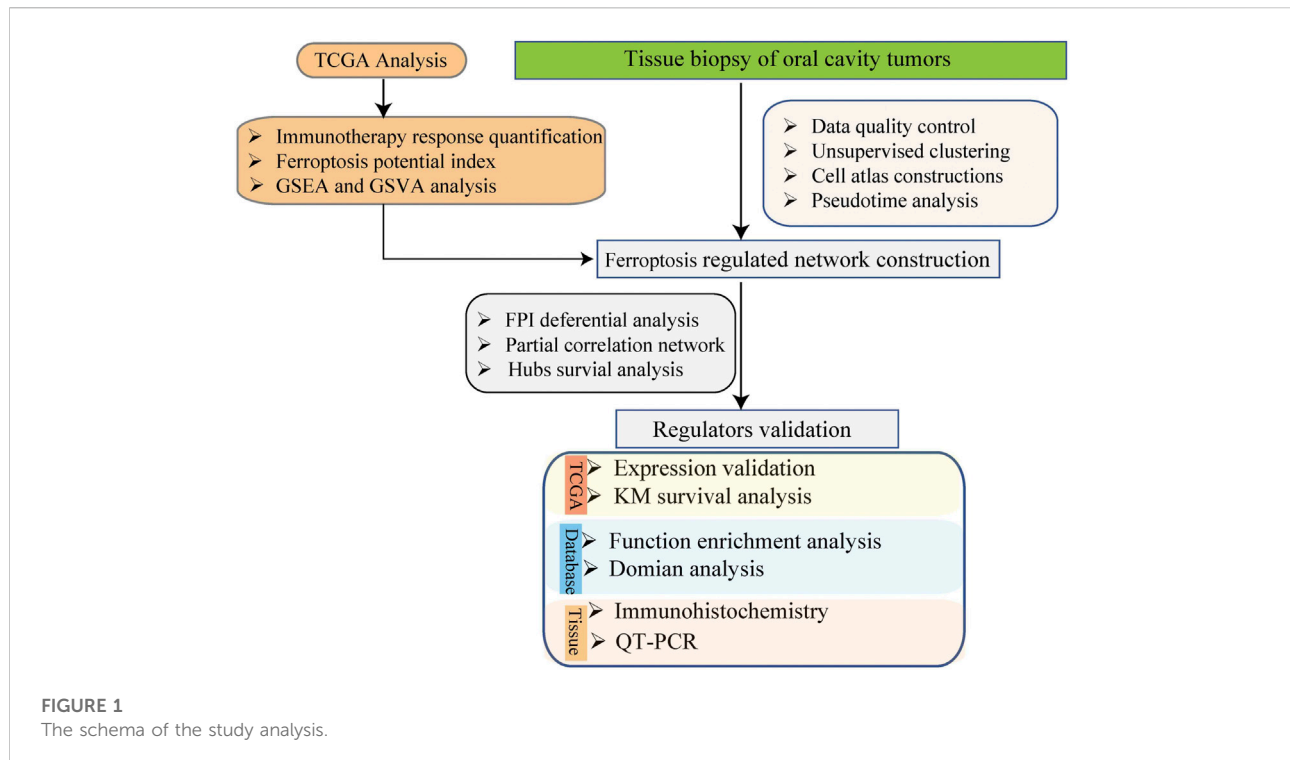
As explained above, there is evidence to demonstrate the role and mechanisms of ferroptosis in several cancers, but the mechanism of the association among HNSCC development and ferroptosis is unclear. In this article, we integrated the single-cell sequencing data and TCGA transcriptome data of HNSCC in order to systematically analyze the relationship between ferroptosis and the prognosis of HNSCC, as well as the related molecular mechanism networks and regulatory molecules, in order to identify markers for targeted treatment of HNSCC.

Materials and methods

Single-cell RNA sequencing analysis

The expression profiling data of 5902 single cells from the tumors of 18 patients with oral cavity tumors were downloaded from the Gene Expression Omnibus database (accession number GSE103322) (Puram et al., 2017). The expression was analyzed with single-cell RNA sequencing (scRNA-seq) using the high-throughput sequencing method Smart-Seq2. The data analysis process is described below. The flow chart of this study analysis shown in Figure 1.

- 1) Quality control of data: The following data filtering parameters were set: minimum number of cells = 3; minimum number of features = 200; mitochondrial gene proportion <0.05; gene count = 200–20,000 (Aran et al., 2019; Kobak and Berens, 2019).
- 2) Unsupervised clustering and construction of a cell Atlas: 1) normalization of the data; 2) screening of genes with high expression variation based on the mean value algorithm; 3) assessment of batch effects across samples by principal component analysis; 4) use of random sampling to construct the background distribution of correlation values between feature genes and principal components in Seurat, and use of the Jackstraw algorithm to select suitable principal components for subsequent cell cluster analysis; 5) use of the k-nearest neighbors algorithm to transform the expression



profiles of cells into highly related cell clusters and identify the clusters (resolution = 0.6); 6) selection of genes that exhibit certain log-fold changes and can be used as markers in most cells based on the following criteria: min.pct = 0.25, logfc.threshold = 0.25 (Kobak and Berens, 2019).

3) Cell cluster definition: SingleR and scCATCH were used to annotate cell clusters (Aran et al., 2019).

Pseudotime analysis

The Monocle algorithm was used to perform developmental trajectory analysis based on highly variable gene sets, and genes with high expression variation in the trajectory were selected for subsequent analysis. The criteria settings were as follows: status = ok; family = tobit; q-value < 0.05; ordering = true (Qiu et al., 2017).

The quantification of immunotherapy response

To calculate the immunophenotypes of tumor-immune cell interactions and the cancer antigenomes, and thus predict the tumor immunotherapy response, the algorithm of Immunophenoscore was used. Here, basing the Immunophenogram algorithm, the weighted averaged Z score were identified, and shown a good predictor of response to immunotherapy, includes anti-cytotoxic T lymphocyte antigen-4

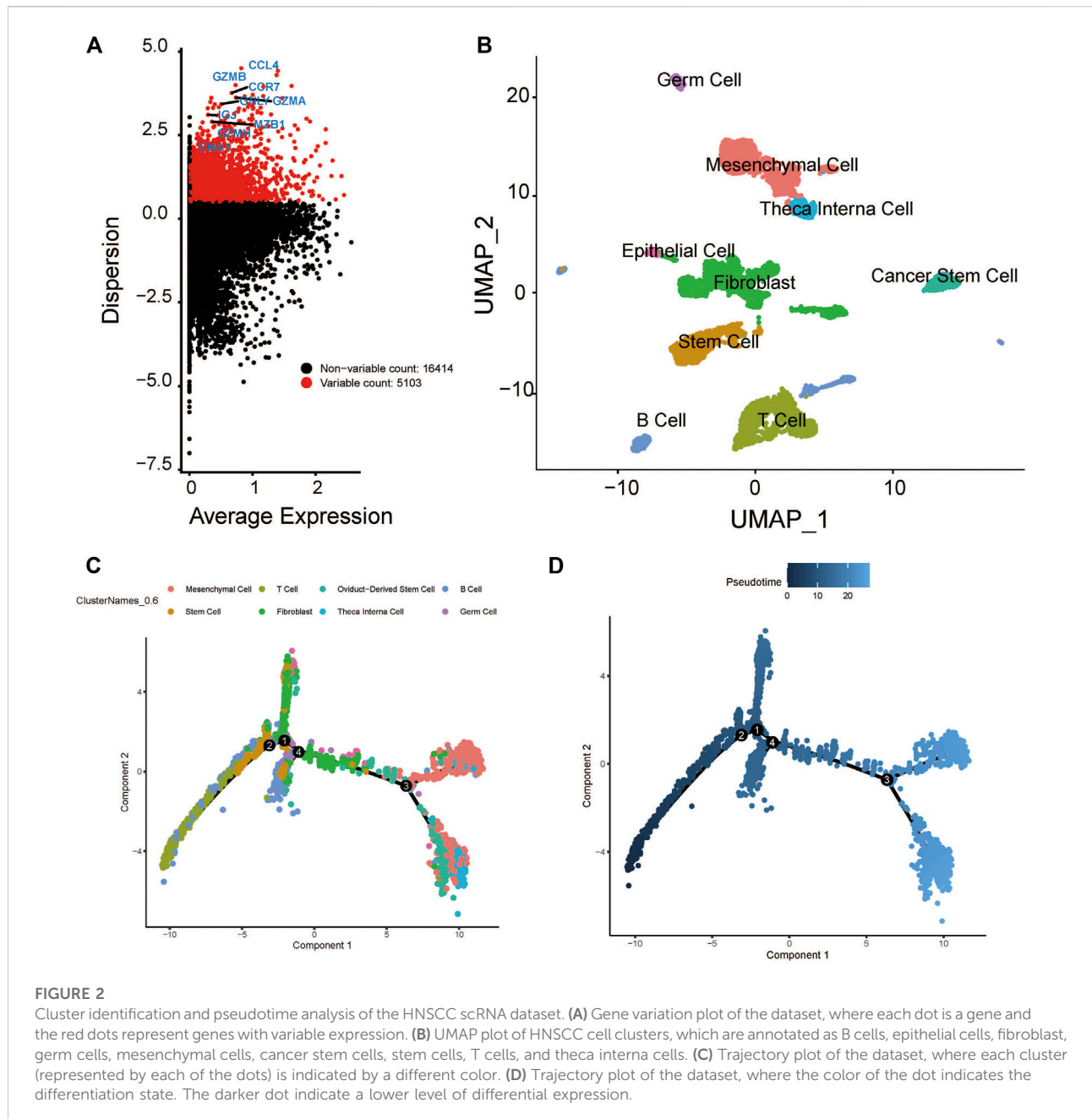
(CTLA-4) and anti-programmed cell death protein 1 (anti-PD-1) antibodies. In addition, the sum of Immunophenoscore (IPS) were calculated by histocompatibility complex (MHC)-related molecules, checkpoints or immunomodulators, effector cells, and suppressor cells (Charoentong et al., 2017).

Correlation analysis of ferroptosis and immunotherapy response

In order to identify the immunotherapy response that were closely associated with ferroptosis, the normalized GSVA scores for ferroptosis and IPS were computed and subjected to Spearman correlation analysis to detect unsupervised clustering (Liberzon et al., 2011; Hänzelmann et al., 2013; Ferreira et al., 2021).

TCGA analysis

The RNA-seq Recompute TPM data, clinical data, and survival data of the GDC TCGA-HNSCC datasets were downloaded from the Xena database at <https://xenabrowser.net/datapages/>. The DESeq algorithm was used to normalize gene expression profiles and filter out low-expression genes. The criteria for selecting differentially expressed genes were as follows: log₂ |fold change| ≥ 1.0; Benjamini-Hochberg (B-H) adjusted *p*-value < 0.05 (Anders and Huber, 2010). While the multiple comparisons were tested by one-way ANOVA,



and the Bonferroni adjusted p -value < 0.05 was considered as significant.

Hub gene identification and functional enrichment analysis

Hub genes were identified based on the intersection of pseudotime analysis-derived differential genes, TCGA-derived differential genes, and ferroptosis pathway genes. Next, functional enrichment analysis and binding protein prediction

were performed on the identified hub genes that were deposited in the Toppgene database at <https://toppgene.cchmc.org/>. The filtering criterion was a false discovery rate-adjusted p -value of < 0.05 (Chen et al., 2009; Liberzon et al., 2011).

Calculation of ferroptosis potential index and survival analysis

Based on Liu et al.'s research, 24 ferroptosis regulator genes were selected and were classified into 1) positive regulators

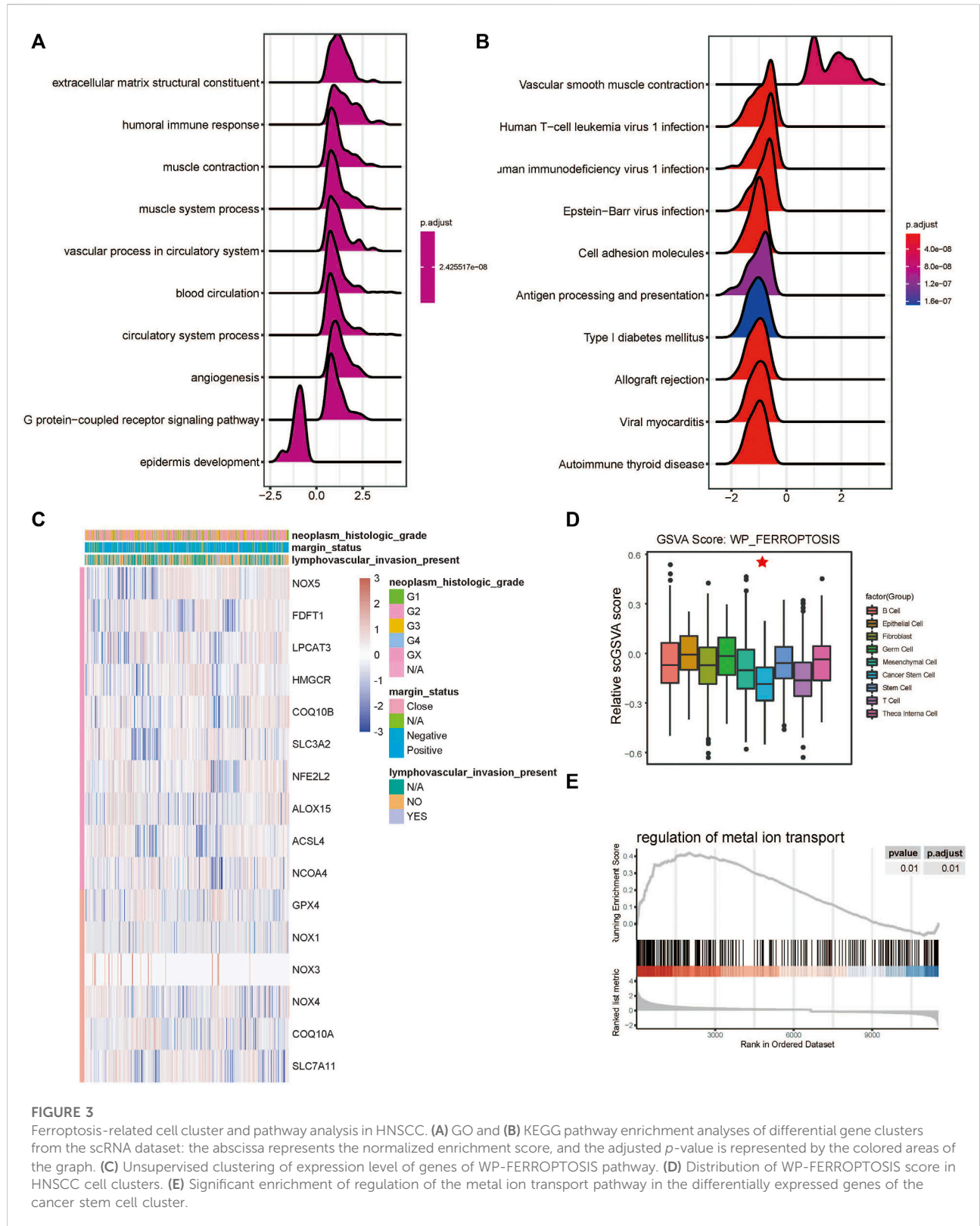
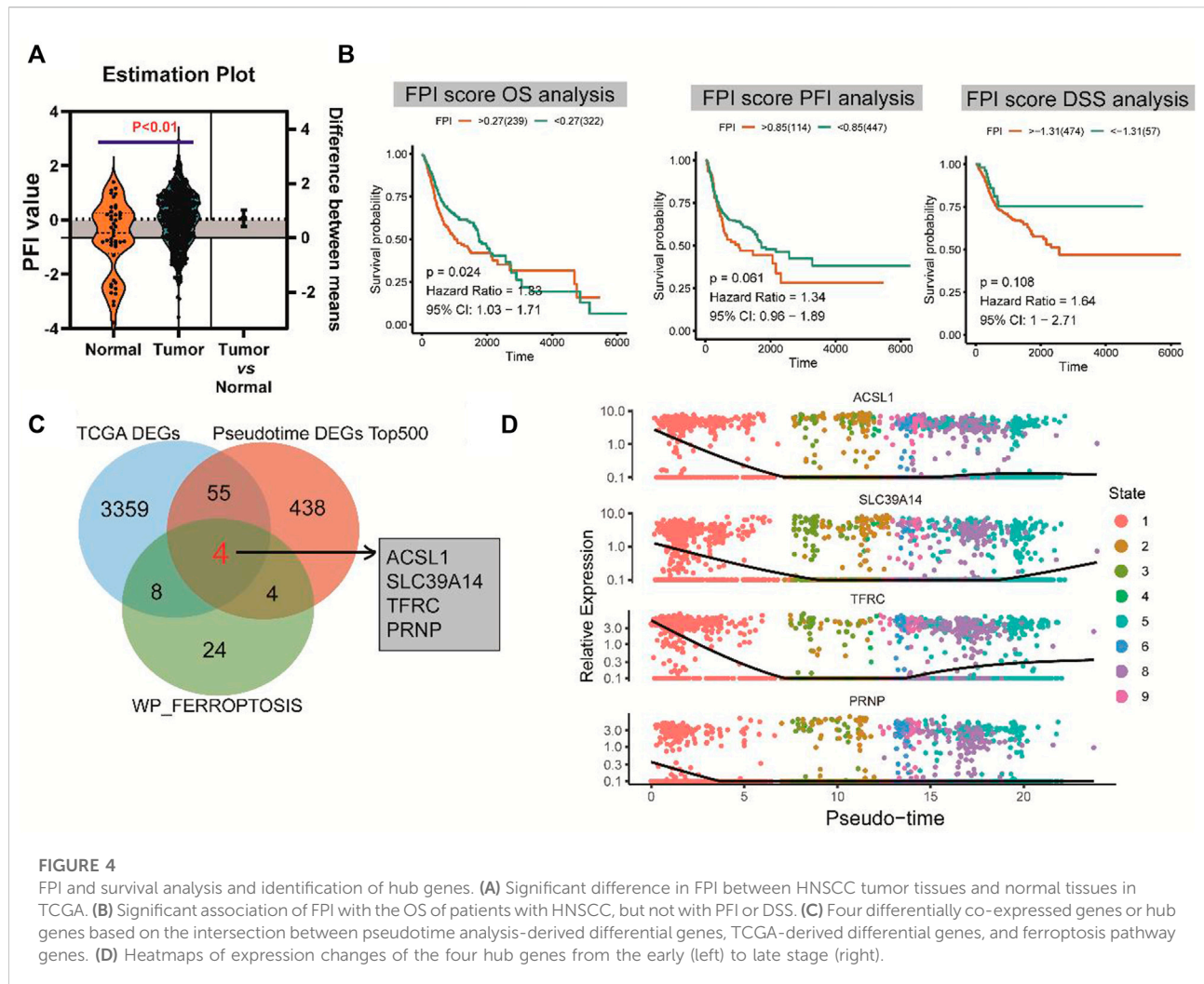


FIGURE 3

Ferroptosis-related cell cluster and pathway analysis in HNSCC. **(A)** GO and **(B)** KEGG pathway enrichment analyses of differential gene clusters from the scRNA dataset: the abscissa represents the normalized enrichment score, and the adjusted *p*-value is represented by the colored areas of the graph. **(C)** Unsupervised clustering of expression level of genes of WP-FERROPTOSIS pathway. **(D)** Distribution of WP-FERROPTOSIS score in HNSCC cell clusters. **(E)** Significant enrichment of regulation of the metal ion transport pathway in the differentially expressed genes of the cancer stem cell cluster.



(LPCAT3, ACSL4, NCOA4, ALOX15, NFE2L2, NOX1, NOX3, NOX4, NOX5, GPX4, SLC3A2, and SLC7A11) and 2) negative regulators (FDFT1, HMGCR, COQ10A, and COQ10B) Liu et al. (2020). The enrichment score (ES) for the positive regulators and the negative regulators was calculated by single-sample gene set enrichment analysis (ssGSEA) in the GSVA package, and ferroptosis potential index (FPI) was calculated as the difference between the two scores. In addition, the survminer package was employed to analyze the relationship of FPI with overall survival (OS), progression-free interval (PFI), and disease-specific survival (DSS).

Pathway enrichment analysis and GSVA

The clusterProfiler package was used to perform gene ontology (GO) analysis, Kyoto Encyclopedia of Genes and Genomes (KEGG) pathway analysis, and reactome pathway analysis on the differentially expressed genes and hub genes

that were identified through pseudotime analysis. B-H adjustment (adjusted p -value, <0.05) was applied to differential pathways. In addition, C2 (curated gene sets), C5 (ontology gene sets), and H (hallmark gene sets) were downloaded from MSigDB at <https://www.gsea-msigdb.org/gsea/msigdb/>, and the GSVA and the GSEABase packages were used for standardized scoring of the gene sets for each cell (Liberzon et al., 2011). The B-H adjusted p -value <0.05 were considered as significant terms in GSVA analysis.

Immunohistochemical staining

All three HNSCC samples and paired non-neoplastic tissues used in immunohistochemical were retrieved from the Department of Pathology, Guangdong Second Provincial General Hospital, China. Before they were used, all cases were diagnosed by three certificated pathologists without discrepancy. This research was conducted under the

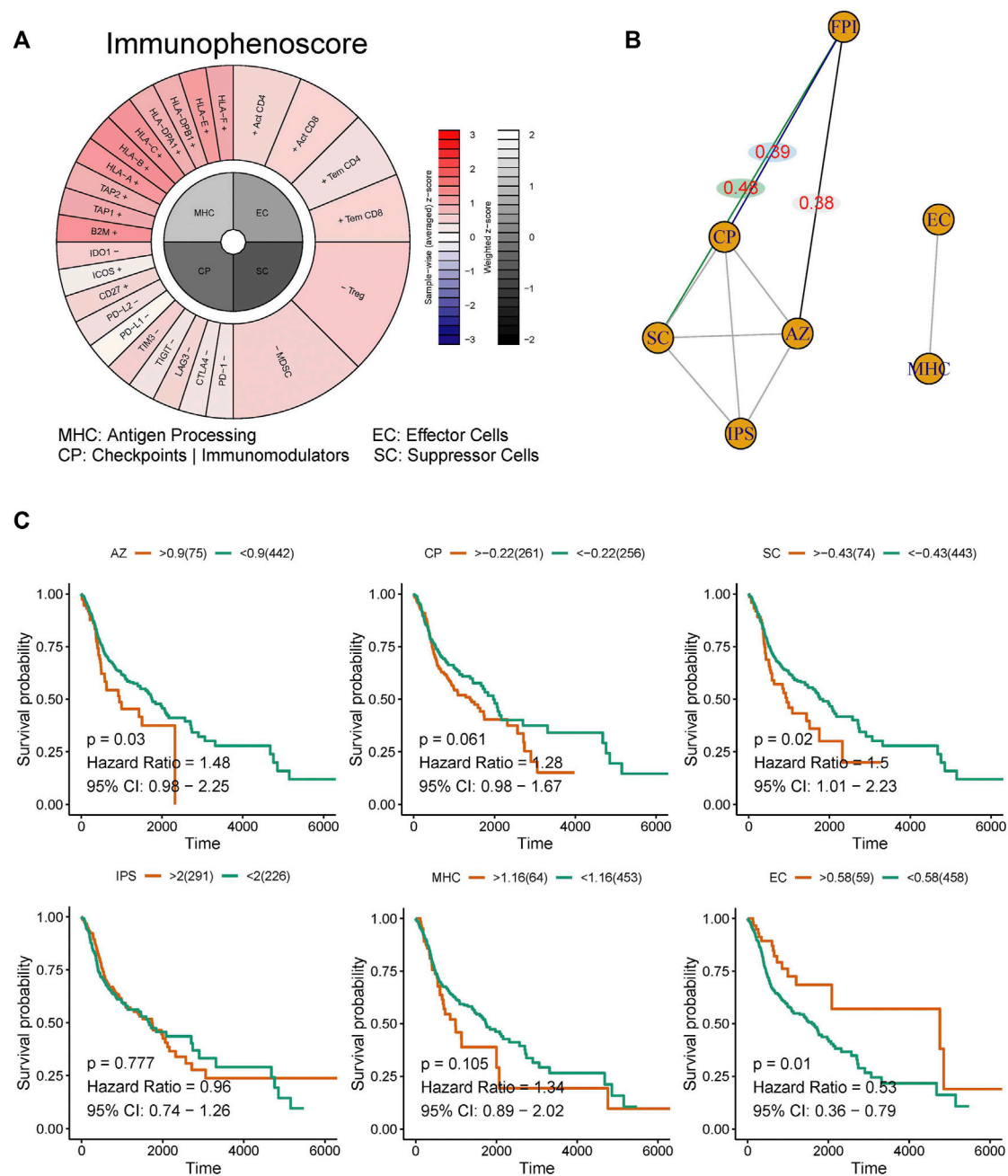
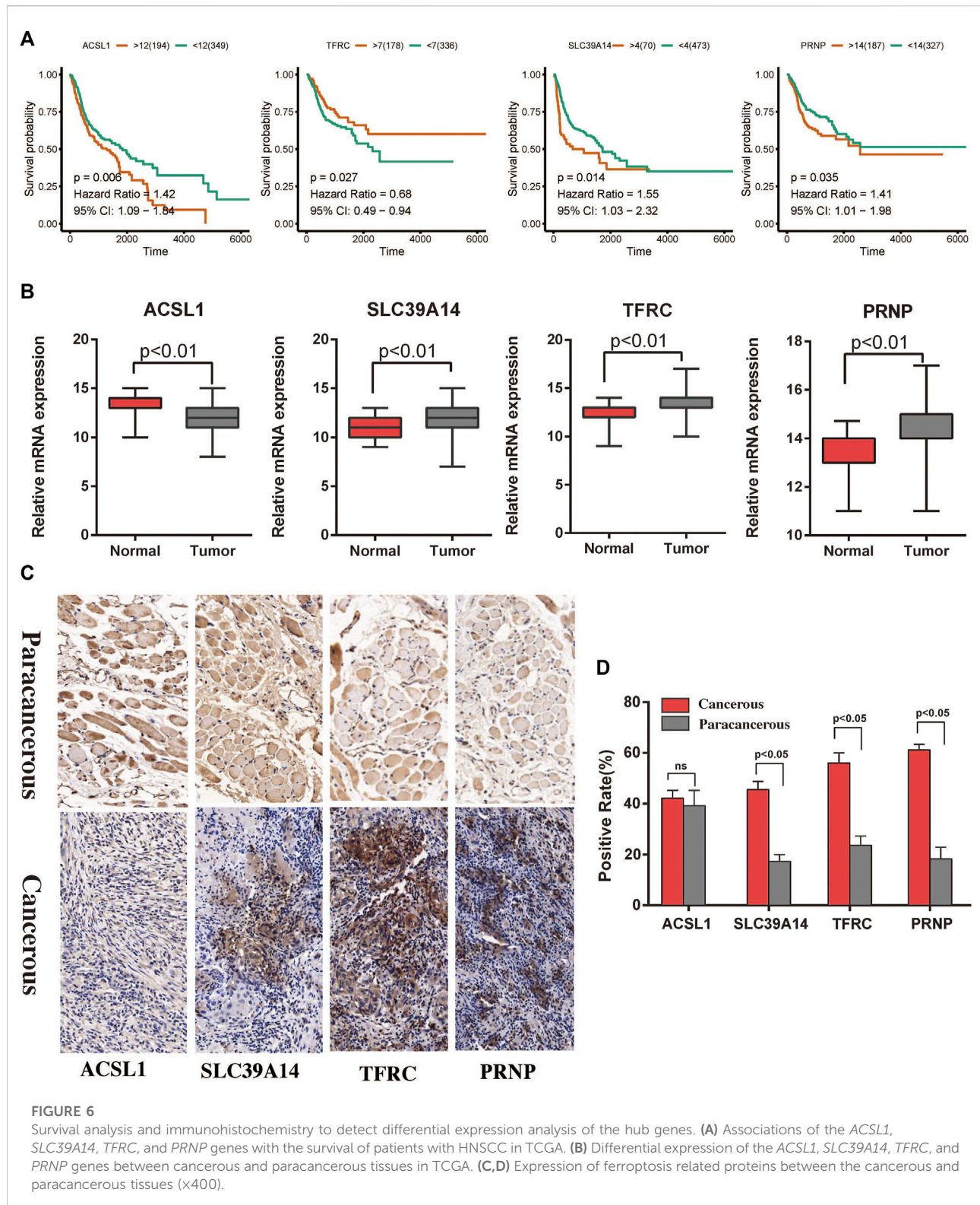


FIGURE 5

Correlation analysis among the ferroptosis pathway and immunotherapy response. (A) The immunophenotypes of tumor-immune landscape were calculated by Immunophenogram algorithm. Significant difference in FPI between HNSCC tumor tissues and normal tissues in TCGA. (B) The partial correlations based on spearman analysis were identified. (C) Survival analysis showed that AZ, SC, and EC were significantly associated with the OS of patients with HNSCC, but not with CP, MHC, and IPS.

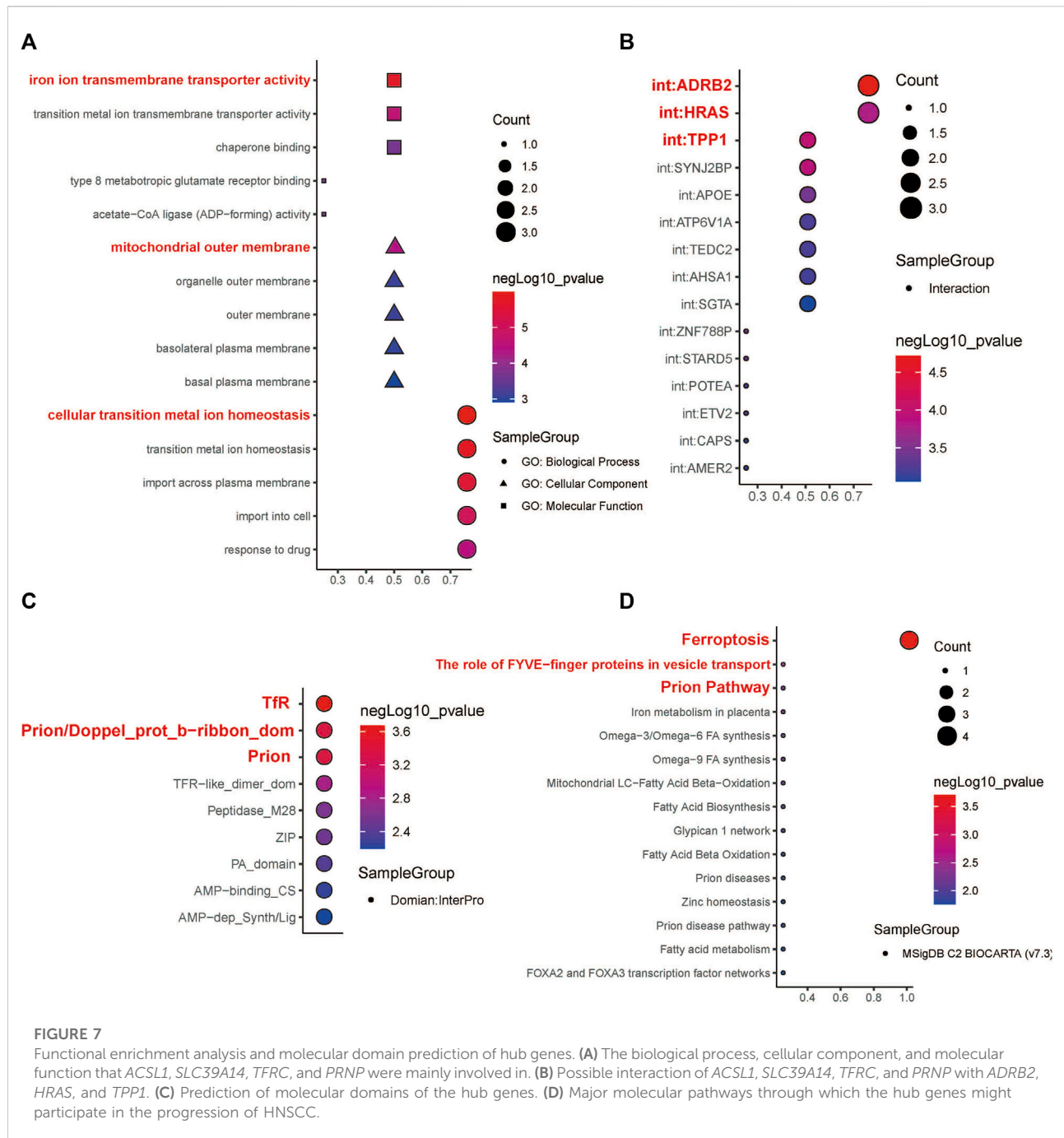
approval and supervision of the Ethics Committee of Guangdong Second Provincial General Hospital. Subsequently, deparaffinized sections were treated with 3% H₂O₂ and subjected to antigen retrieval by citric acid (pH6.0). After overnight incubation with primary antibody

(anti-ACSL1, anti-SLC39A14, anti-TFRC and PRNP antibody (Proteintech Group, China) by 1:200 at 4°C, sections were incubated for 15 min at room temperature with horseradish peroxidase-labeled polymer conjugated with secondary antibody (MaxVision Kits) and incubated for 1 min with



diaminobenzidine. The sections were then lightly counterstained with hematoxylin. The sections without primary antibody were served as negative controls.

Expression area of ACSL1, SLC39A14, TFRC and PRNP was determined according to the Image J (<https://imagej.net/software/fiji/downloads>; Life-Line versions).



Results

Single-cell RNA-sequencing analysis

After quality control, the single-cell transcriptomic data of 5902 cells from 18 patients with oral cavity tumors were obtained. Unsupervised clustering was performed on merged datasets after normalization and correction. Cells were annotated with marker genes of known cell types. A

total of 5103 genes with variable expression were identified, including *GZMB*, *GNLY*, *MZB1*, *CCR7*, and *CCL4* (Figure 2A). Using t-distributed stochastic neighbor embedding and uniform manifold approximation and projection for dimension reduction, 5902 cell clusters were identified, including B cells, epithelial cells, fibroblasts, germ cells, mesenchymal cells, cancer stem cells, stem cells, T cells, and theca interna cells. The distribution of cells was plotted in a two-dimensional space (Figure 2B).

Pseudotime analysis and enrichment analysis

The expression profiles of cells were projected onto a low-dimensional space to construct a differentiation trajectory of cells, wherein cells of similar states were aggregated together. There were four branching points along the differentiation trajectory of HNSCC that represented potential decision points of the cellular biological process (Figures 2C,D).

The developmental trajectory analysis was performed on highly variable gene sets. Following log normalization and dimension reduction using the DDRTree algorithm, differentially regulated genes, after B-H adjustment in the pseudotime analysis, were selected for subsequent functional enrichment analyses. GO analysis showed that the following pathways were associated with the differentiation and progression of HNSCC: extracellular matrix structural constituent (ES = 0.56, normalized ES [NES] = 2.61, P.adjust = 1.00E-10), humoral immune response (ES = 0.54, NES = 2.71, P.adjust = 1.00E-10), and muscle contraction (ES = 0.51, NES = 2.69, P.adjust = 1.00E-10) (Figure 3A). KEGG analysis revealed that the following pathways were significantly enriched: vascular smooth muscle contraction (ES = 0.55, NES = 2.58, P.adjust = 1.44E-9), human T-cell leukemia virus one infection (ES = -0.34, NES = -2.52, P.adjust = 1.00E-10), and human immunodeficiency virus one infection (ES = -0.35, NES = -2.64, P.adjust = 1.00E-10) (Figure 3B). In addition, we draw a heatmap prototype for showing the expression level of genes in ferroptosis pathway (Figure 3C). Among all the cell clusters of HNSCC, the cancer stem cell cluster showed the lowest expression and highest variation in the FERROPTOSIS pathway and, therefore, was considered as the FERROPTOSIS-related core cell cluster (Figure 2D). Further, the regulation of the metal ion transport pathway was significantly enriched in the differentially expressed genes of the cancer stem cell cluster (ES = 0.42, NES = 2.24, P.adjust = 5.97E-10) (Figure 3E).

Ferroptosis potential index and survival analysis and identification of hub genes

FPI was calculated for each HNSCC sample in the TCGA database based on the method described by Liu et al. (2022). There was a significant difference in FPI between HNSCC tumor tissues and normal tissues ($p < 0.01$) (Figure 4A). With the survminer package and survival R package, patients with HNSCC were divided into high and low expression groups. Survival analysis showed that FPI was significantly associated with the OS of patients with HNSCC [$p = 0.024$, hazard ratio = 1.33, 95% confidence interval (CI) = 1.03–1.71], but not with PFI ($p = 0.061$,

hazard ratio = 1.34, 95% CI = 0.96–1.89), or DSS ($p = 0.108$, hazard ratio = 1.64, 95% CI = 1–2.71) (Figure 4B).

A total of four differentially co-expressed genes, or hub genes, were identified based on the intersection of pseudotime analysis-derived differentially expressed genes, TCGA-derived differentially expressed genes, and FERROPTOSIS pathway genes: ACSL1, SLC39A14, TFRC, and PRNP (Figure 4C). The results of pseudotime analysis indicated that these four hub genes exhibited consistent expression changes in the differentiation process of HNSCC (Figure 4D).

Correlation between the ferroptosis pathway and immunotherapy response

The scores for WP-FERROPTOSIS and IPS were quantified (Figure 5A). Unsupervised clustering based on the correlation coefficients according to Spearman correlation analysis revealed close correlations between WP-FERROPTOSIS and antigen processing of MHC, effector cells (EC), immunomodulators of checkpoints (CP, correlation coefficient = 0.39, $p = 0.04$), suppressor cells (SC, correlation coefficient = 0.48, $p = 0.03$), and averaged Z (AZ, correlation coefficient = 0.38, $p = 0.04$) score (Figure 5B). Survival analysis showed that AZ [$p = 0.03$, hazard ratio = 1.48, 95% confidence interval (CI) = 0.98–2.25], SC ($p = 0.02$, hazard ratio = 1.50, 95% CI = 1.01–2.23), and EC ($p = 0.01$, hazard ratio = 0.53, 95% CI = 0.36–0.79) were significantly associated with the OS of patients with HNSCC, but not with CP ($p = 0.06$, hazard ratio = 1.28, 95% CI = 0.98–1.67), MHC ($p = 0.11$, hazard ratio = 1.34, 95% CI = 0.89–2.02), and IPS ($p = 0.78$, hazard ratio = 0.96, 95% CI = 0.74–1.26) (Figure 5C).

Survival analysis and functional enrichment analysis of the hub genes

The expression levels of the four hub genes were significantly associated with the survival of patients with HNSCC (Figure 6A). They also showed significantly different expression levels between the cancer tissues and the para-cancerous tissues of patients with HNSCC (Figure 6B). Our results indicated that SLC39A14, TFRC and PRNP are up-regulated in most HNSCC patients. However, there was no significant difference in the expression of ACSL1 (Figures 6C,D). The iron ion transmembrane transporter activity, mitochondrial outer membrane, and cellular transition metal ion homeostasis pathways were significantly enriched in the four hub genes (Figure 7A). Further, exploration of the biological mechanisms indicated that the hub genes may exert their effects in HNSCC through interactions with the *ADRB2*, *HRAS*, and *TPPI* genes (Figure 7B).

Hub gene interaction and molecular domain prediction

According to the InterPro database, Tfr, Prion/Doppel_prot_b-ribbon_dom, and Prion are likely to be the molecular domains of the four hub genes (Figure 7C). The four hub genes were mainly enriched in the following Biocarta pathways: Ferroptosis, The role of FYVE-finger proteins in vesicle transport, and Prion Pathway (Figure 7D).

Discussion

The current study explores the role and mechanisms of the ferroptosis pathway in HNSCC, as ferroptosis is an important inhibitory mechanism in tumor cells. We believe that the findings shed light on the underlying ferroptosis-related mechanisms of HNSCC and can help in the identification of molecular markers that could accurately predict the outcome of HNSCC. These findings could eventually have immense clinical value for the treatment and prognosis of HNSCC.

Our results indicate that the ferroptosis pathway is closely associated with the overall survival of patients with HNSCC, and it is mainly involved in the regulation of extracellular matrix structure, humoral immune response, and vascular smooth muscle contraction. Additionally, it was found that ferroptosis pathway changes mainly occur in cancer stem cells, in comparison to other cell types; additionally, changes in the metal ion transport pathway were also significant in cancer cells. The latter finding supports the role of ferroptosis in HNSCC, as ferroptosis is induced by lipid ROS, which are largely generated by enzymes that contain iron or iron derivatives such as ferroheme and heme oxygenase-1.

According to the present findings, the expression levels of four genes, namely, *ACSL1*, *SLC39A14*, *TFRC*, and *PRNP*, were closely linked with ferroptosis, the occurrence of HNSCC, and the long-term outcome of patients. These genes are, therefore, potential targets for the development, progression, and treatment of HNSCC. Zhang et al. (2021) found that the higher expression level of *ACSL1* could activate fatty-acid (FA) metabolic reprogramming during ovarian cancer metastasis and convert the lipid profile via AMP-activated protein kinase and Src pathways. Guo et al. (2020), demonstrated that the Acyl-CoA synthetase long-chain family member 1 (*ACSL1*) is an oncogene in thyroid cancers, and the higher expression level of *ACSL1* led to a suppression of cancer cell progression and migration. Thomas et al. (2019), the activity of *ACSL1* could convert the TNF α mediates inflammatory responses via attenuates the phosphorylation of p38 MAPK, ERK1/2, and NF- κ B in breast cancer. Thorsen et al. (2011), illustrated that the alternative splicing of *SLC39A14* is significantly difference among the adenomas and cancers, especially in the mutation of exclusive exons 4A, 4B, and the exon 4A/4B ratio. Wang et al. (2018),

found that the expression level of *SLC39A14* significantly correlated with the weightlessness of skeletal muscle mass and cachexia via regulated with zinc uptake in muscle progenitor cells. Xu et al. (2016), demonstrated that the lower expression level of *SLC39A14* protein may significantly correlated with a higher Gleason score, advanced clinical stage, presence of metastasis, and prostate-specific antigen failure in human prostate cancer. Wu et al. (2019), reported that *TFRC* play a key role in cancer cellular metabolism and proto-oncogenic transcription via regulated by NF2-YAP signaling axis. *TFRC* regard as the key transporter in the intracellular iron, and the higher expression level of increased *TFRC* was associated with a worse prognosis for epithelial ovarian cancer patients (Huang et al., 2020). Stewart et al. (2019), shown that the expression level of TP63, PSAT1, and *TFRC* may correlated with the function of oxidation-reduction and glutathione in squamous cell lung cancer. Santos et al. (2021), found that the expression level of *PRNP* may significantly correlated with lymph node metastasis progression and worse prognosis for patients with head and neck squamous cell carcinoma. López-Cortés et al. (2020), demonstrated that the protein of *PRNP*, *S100A9*, *DDA1*, *TXN*, *RPS27*, *S100A14*, *S100A7*, *MAPK1*, *AGR3* and *NDUFA13* were considered as the best ranked metastasis driver proteins. AS an evolutionarily conserved cell surface protein, the higher expression level of *PRNP* closely related with the acquisition of malignant feature of cancer stem cells of multiple cancers, includes glioblastoma multiforme, breast cancer, and gastric cancer (Ryskalin et al., 2019).

In this study, the GSVA score for the ferroptosis pathway was closely correlated with the OS of patients with HNSCC, had a potential correlation with the PFI, and had no significant correlation with DSS. These findings indicate that HNSCC cells might escape ferroptosis through a balance of iron and thiol redox signaling. However, more research is required in the future to clarify the relationship between iron pathways, ferroptosis, and the origin of HNSCC.

Conclusion

In summary, the ferroptosis pathway is closely associated with the development and progression of HNSCC, possibly through regulation of cancer stem cell proliferation. The *ACSL1*, *SLC39A14*, *TFRC*, and *PRNP* genes may be critical for ferroptosis-related development and progression of HNSCC, and may serve as potential treatment targets. These informative protein domains might be used in novel strategies for developing effective therapies targeting HNSCC. These findings also allow a better understanding of the molecular mechanisms involved in HNSCC development, thereby enabling the exploration of ferroptosis-related pathophysiology from a new perspective, and thus may raise current therapies to a new standard. Although these results are encouraging, we

currently do not understand how hub regulators contributing to HNSCC development or which regulators with clinical transformation value, that improved prognostic outcomes. Thus, the further confirmed is required and necessary, based on animal models and large sample clinical verification, for the above analysis results.

Data availability statement

The datasets presented in this study can be found in online repositories. The names of the repository/repositories and accession number(s) can be found below: GEO with accession GSE103322.

Ethics statement

The studies involving human participants were reviewed and approved by The Ethics Committee of Guangdong Second Provincial General Hospital. The patients/participants provided their written informed consent to participate in this study.

Author contributions

FL conceived and conceptualized the project, acquired data, and wrote the draft manuscript. LT and QL were responsible for

methodology and software. JT, JH, and ZY were responsible for writing, reviewing and editing. All authors read, edited several draft versions, and approved the final manuscript.

Funding

This research was supported financially by the Doctoral workstation foundation of Guangdong Second Provincial General hospital (No. 2021BSH001); Funding by Science and Technology Projects in Guangzhou (No. 20212020298).

Conflict of interest

The authors declare that the research was conducted in the absence of any commercial or financial relationships that could be construed as a potential conflict of interest.

Publisher's note

All claims expressed in this article are solely those of the authors and do not necessarily represent those of their affiliated organizations, or those of the publisher, the editors and the reviewers. Any product that may be evaluated in this article, or claim that may be made by its manufacturer, is not guaranteed or endorsed by the publisher.

References

- Anders, S., and Huber, W. (2010). Differential expression analysis for sequence count data. *Genome Biol.* 11 (10), R106. doi:10.1186/gb-2010-11-10-r106
- Aran, D., Looney, A. P., Liu, L., Wu, E., Fong, V., Hsu, A., et al. (2019). Reference-based analysis of lung single-cell sequencing reveals a transitional profibrotic macrophage. *Nat. Immunol.* 20 (2), 163–172. doi:10.1038/s41590-018-0276-y
- Cao, J. Y., and Dixon, S. J. (2016). Mechanisms of ferroptosis. *Cell. Mol. Life Sci.* 73 (11–12), 2195–2209. doi:10.1007/s00018-016-2194-1
- Chen, J., Bardes, E. E., Aronow, B. J., and Jegga, A. G. (2009). ToppGene Suite for gene list enrichment analysis and candidate gene prioritization. *Nucleic Acids Res.* 37, W305–W311. Web Server issue. doi:10.1093/nar/gkp427
- Chen, Z., Li, Z., Li, C., Huang, H., Ren, Y., Li, Z., et al. (2022). Manganese-containing polydopamine nanoparticles as theranostic agents for magnetic resonance imaging and photothermal/chemodynamic combined ferroptosis therapy treating gastric cancer. *Drug Deliv.* 29 (1), 1201–1211. doi:10.1080/10717544.2022.2059124
- Ferreira, M. R., Santos, G. A., Biagi, C. A., Silva Junior, W. A., and Zambuzzi, W. F. (2021). GSVA score reveals molecular signatures from transcriptomes for biomaterials comparison. *J. Biomed. Mat. Res. A* 109 (6), 1004–1014. doi:10.1002/jbm.a.37090
- Guo, L., Lu, J., Gao, J., Li, M., Wang, H., Zhan, X., et al. (2020). The function of SNHG7/miR-449a/ACSL1 axis in thyroid cancer. *J. Cell. Biochem.* 121 (10), 4034–4042. doi:10.1002/jcb.29569
- Hamman, J., Howe, C. L., Borgstrom, M., Baker, A., Wang, S. J., Bearely, S., et al. (2021). Impact of close margins in head and neck mucosal squamous cell carcinoma: A systematic review. *Laryngoscope* 132, 307–321. doi:10.1002/lary.29690
- Hänzelmann, S., Castelo, R., and Guinney, J. (2013). Gsva: gene set variation analysis for microarray and RNA-seq data. *BMC Bioinforma.* 14, 7. doi:10.1186/1471-2105-14-7
- Huang, S., Le, H., Hong, G., Chen, G., Zhang, F., Lu, L., et al. (2022). An all-in-one biomimetic iron-small interfering RNA nanoplatform induces ferroptosis for cancer therapy. *Acta Biomater.* S1742-7061, 00357–00359. doi:10.1016/j.actbio.2022.06.017
- Huang, Y., Huang, J., Huang, Y., Gan, L., Long, L., Pu, A., et al. (2020). TFRC promotes epithelial ovarian cancer cell proliferation and metastasis via up-regulation of AXIN2 expression. *Am. J. Cancer Res.* 10 (1), 131–147.
- Jing, F. Y., Zhou, L. M., Ning, Y. J., Wang, X. J., and Zhu, Y. M. (2021). The biological function, mechanism, and clinical significance of m6A RNA modifications in head and neck carcinoma: A systematic review. *Front. Cell Dev. Biol.* 9, 683254. doi:10.3389/fcell.2021.683254
- Kobak, D., and Berens, P. (2019). The art of using t-SNE for single-cell transcriptomics. *Nat. Commun.* 10 (1), 5416. doi:10.1038/s41467-019-13056-x
- Liang, C., Zhang, X., Yang, M., and Dong, X. (2019). Recent progress in ferroptosis inducers for cancer therapy. *Adv. Mat.* 31 (51), e1904197. doi:10.1002/adma.201904197
- Liberzon, A., Subramanian, A., Pinchback, R., Thorvaldsdóttir, H., Tamayo, P., Mesirov, J. P., et al. (2011). Molecular signatures database (MSigDB) 3.0. *Bioinformatics* 27 (12), 1739–1740. doi:10.1093/bioinformatics/btr260
- Liu, Z., Zhao, Q., Zuo, Z. X., Yuan, S. Q., Yu, K., Zhang, Q., et al. (2020). Systematic analysis of the aberrances and functional implications of ferroptosis in cancer. *iScience* 23 (7), 101302. doi:10.1016/j.isci.2020.101302
- López-Cortés, A., Cabrera-Andrade, A., Vázquez-Naya, J. M., Pazos, A., González-Díaz, H., Paz, Y. M. C., et al. (2020). Prediction of breast cancer proteins involved in immunotherapy, metastasis, and RNA-binding using molecular descriptors and artificial neural networks. *Sci. Rep.* 10 (1), 8515. doi:10.1038/s41598-020-65584-y

- Magesh, S., and Cai, D. (Forthcoming 2022). Roles of YAP/TAZ in ferroptosis. *Trends Cell Biol.* S0962-8924, 00136–142. doi:10.1016/j.tcb.2022.05.005
- Membreno, P. V., Luttrell, J. B., Mamidala, M. P., Schwartz, D. L., Hayes, D. N., Gleysteen, J. P., et al. (2021). Outcomes of primary radiotherapy with or without chemotherapy for advanced oral cavity squamous cell carcinoma: Systematic review. *Head. Neck* 43, 3165–3176. doi:10.1002/hed.26779
- Peng, H., Zhang, X., Yang, P., Zhao, J., Zhang, W., Feng, N., et al. (2023). Defect self-assembly of metal-organic framework triggers ferroptosis to overcome resistance. *Bioact. Mat.* 19, 1–11. doi:10.1016/j.bioactmat.2021.12.018
- Puram, S. V., Tirosh, I., Parikh, A. S., Patel, A. P., Yizhak, K., Gillespie, S., et al. (2017). Single-cell transcriptomic analysis of primary and metastatic tumor ecosystems in head and neck cancer. *Cell* 171 (7), 1611–1624. e1624. doi:10.1016/j.cell.2017.10.044
- Qiu, X., Mao, Q., Tang, Y., Wang, L., Chawla, R., Pliner, H. A., et al. (2017). Reversed graph embedding resolves complex single-cell trajectories. *Nat. Methods* 14 (10), 979–982. doi:10.1038/nmeth.4402
- Ryskalin, L., Busceti, C. L., Biagioni, F., Limanaqi, F., Familiari, P., Frati, A., et al. (2019). Prion protein in glioblastoma multiforme. *Int. J. Mol. Sci.* 20 (20), E5107. doi:10.3390/ijms20205107
- Sacco, A. G., Chen, R., Worden, F. P., Wong, D. J. L., Adkins, D., Swiecicki, P., et al. (2021). Pembrolizumab plus cetuximab in patients with recurrent or metastatic head and neck squamous cell carcinoma: An open-label, multi-arm, non-randomised, multicentre, phase 2 trial. *Lancet. Oncol.* 22 (6), 883–892. doi:10.1016/s1470-2045(21)00136-4
- Santos, E. M., Fraga, C. A. C., Xavier, A., Xavier, M. A. S., Souza, M. G., Jesus, S. F., et al. (2021). Prion protein is associated with a worse prognosis of head and neck squamous cell carcinoma. *J. Oral Pathol. Med.* 50, 985–994. doi:10.1111/jop.13188
- Stewart, P. A., Welsh, E. A., Slebos, R. J. C., Fang, B., Izumi, V., Chambers, M., et al. (2019). Proteogenomic landscape of squamous cell lung cancer. *Nat. Commun.* 10 (1), 3578. doi:10.1038/s41467-019-11452-x
- Thomas, R., Al-Rashed, F., Akhter, N., Al-Mulla, F., and Ahmad, R. (2019). ACSL1 regulates tnfa-induced GM-CSF production by breast cancer MDA-MB-231 cells. *Biomolecules* 9 (10), E555. doi:10.3390/biom9100555
- Thorsen, K., Mansilla, F., Schepeler, T., Øster, B., Rasmussen, M. H., Dyrskjøt, L., et al. (2011). Alternative splicing of SLC39A14 in colorectal cancer is regulated by the Wnt pathway. *Mol. Cell. Proteomics* 10 (1), M110002998. doi:10.1074/mcp.M110.002998
- Wang, G., Biswas, A. K., Ma, W., Kandpal, M., Coker, C., Grandgenett, P. M., et al. (2018). Metastatic cancers promote cachexia through ZIP14 upregulation in skeletal muscle. *Nat. Med.* 24 (6), 770–781. doi:10.1038/s41591-018-0054-2
- Wu, J., Minikes, A. M., Gao, M., Bian, H., Li, Y., Stockwell, B. R., et al. (2019). Intercellular interaction dictates cancer cell ferroptosis via NF2-YAP signalling. *Nature* 572 (7769), 402–406. doi:10.1038/s41586-019-1426-6
- Xie, Y., Xiao, Y., Liu, Y., Lu, X., Wang, Z., Sun, S., et al. (2022). Construction of a novel radiosensitivity- and ferroptosis-associated gene signature for prognosis prediction in gliomas. *J. Cancer* 13 (8), 2683–2693. doi:10.7150/jca.72893
- Xu, X. M., Wang, C. G., Zhu, Y. D., Chen, W. H., Shao, S. L., Jiang, F. N., et al. (2016). Decreased expression of SLC39A14 is associated with tumor aggressiveness and biochemical recurrence of human prostate cancer. *Oncotargets. Ther.* 9, 4197–4205. doi:10.2147/ott.S103640
- Yang, W. S., and Stockwell, B. R. (2016). Ferroptosis: Death by lipid peroxidation. *Trends Cell Biol.* 26 (3), 165–176. doi:10.1016/j.tcb.2015.10.014
- Zhai, F. G., Liang, Q. C., Wu, Y. Y., Liu, J. Q., and Liu, J. W. (2022). Red ginseng polysaccharide exhibits anticancer activity through GPX4 downregulation-induced ferroptosis. *Pharm. Biol.* 60 (1), 909–914. doi:10.1080/13880209.2022.2066139
- Zhang, H., Zhuo, Y., Li, D., Zhang, L., Gao, Q., Yang, L., et al. (2022). Dihydroartemisinin inhibits the growth of pancreatic cells by inducing ferroptosis and activating antitumor immunity. *Eur. J. Pharmacol.* 926, 175028. doi:10.1016/j.ejphar.2022.175028
- Zhang, Q., Zhou, W., Yu, S., Ju, Y., To, S. K. Y., Wong, A. S. T., et al. (2021). Metabolic reprogramming of ovarian cancer involves ACSL1-mediated metastasis stimulation through upregulated protein myristoylation. *Oncogene* 40 (1), 97–111. doi:10.1038/s41388-020-01516-4